Absorption spectroscopy and imaging from the visible through mid-infrared with 20 nm resolution.

Aaron M. Katzenmeyer,[1] Glenn Holland,[1] Kevin Kjoller[2] and Andrea Centrone[1]*

[1]Center for Nanoscale Science and Technology, National Institute of Standards and Technology, 100 Bureau Drive, Gaithersburg, Maryland 20899, United States.
[*]E-mail: andrea.centrone@nist.gov

[2]Anasys Instruments, Inc., 325 Chapala Street, Santa Barbara, California 93101, United States.

Abstract

Absorption spectroscopy and mapping from visible through mid-IR wavelengths has been achieved with spatial resolution exceeding the limit imposed by diffraction, via the photothermal induced resonance technique. Correlated vibrational (chemical), and electronic properties are obtained simultaneously with topography with a wavelength-independent resolution of ≈ 20 nm using a single laboratory-scale instrument. This marks the highest resolution reported for PTIR, as determined by comparing height and PTIR images, and its first extension to near-IR and visible wavelengths.

Light-matter interaction enables scientists to characterize materials and biological samples across a large range of energies. Visible (VIS) and near-infrared (NIR) light (from 400 nm to 2.5 μm) probes electronic transitions in materials [1], providing information regarding band gap, defects, and energy transfer which is crucial for the semiconductor and optoelectronic industries and for understanding processes such as photosynthesis. Mid-infrared (mid-IR) light (from 2.5 μm to 15 μm) probes vibrational transitions and provides rich chemical and structural information enabling materials identification [2]. Spectral maps can be obtained by coupling a light source and a spectrometer with an optical microscope [3]. However, light diffraction limits the lateral resolution achievable with conventional microscopic techniques to approximately half the wavelength of light [4]. This limitation has two drawbacks: first, the lateral resolution is insufficient to measure nanomaterials at commensurate length scales (particularly in the mid-IR) and second, the wavelength-dependent resolution impedes comparison of spectral maps from different spectral ranges. Super resolution techniques such as stimulated emission depletion (STED) microscopy [5], photoactivated localization microscopy (PALM) [6],stochastic optical reconstruction microscopy (STORM) [7], and others allow imaging with a lateral resolution that

surpasses the optical diffraction limit. Because of the high spatial resolution (down to a few nanometers [6]), fast acquisition and the ability to provide 3-dimentional images of the sample, these techniques are extremely useful for imaging biological samples. However, super resolution techniques typically rely on extrinsic fluorescent labels and do not provide intrinsic properties of the sample.

Scattering scanning near-field optical microscopy (s-SNOM) [8,9] measures the amplitude and phase of light scattering from a sharp tip in proximity to the sample. s-SNOM has been implemented at selected visible and terahertz wavelengths [10], however absorption spectra in these ranges have not yet been reported. Because of the availability of wavelength-tunable laser sources in the mid-IR, s-SNOM can in principle provide IR absorption spectra that are directly related to the intrinsic chemical composition of the sample [11,12]. However, in general the scattered light is not a simple function of absorption but depends also on the real part of the sample's index of refraction (i.e. scattering) and may also depend on extrinsic parameters concerning the substrate and the tip [13,14]. Consequently, s-SNOM spectra do not always correlate with far-field IR spectra [12] and may require a tip-specific model [13] for retrieving the intrinsic properties of the sample (i. e. its chemical composition).

Photothermal induced resonance (PTIR) [15-19], also known as AFM-IR, employs a pulsed wavelength-tunable laser for sample illumination and an AFM tip to locally transduce the absorbed energy into cantilever oscillations via the thermal expansion of the sample. The intensity of the PTIR signal is independent of scattering and proportional to the absorbed energy [17] thus enabling material identification via direct comparison of PTIR spectra with far-field IR spectral libraries [20]. To date, PTIR has been restricted to the mid-IR spectral range. In this work we integrate a laser tunable from 400 nm to 2.30 µm into a commercial PTIR setup and acquire absorption spectra and maps with ≈ 20 nm resolution over a spectral range spanning from 500 nm to 16 µm. As proof of principle we assess the homogeneity of dye-loaded poly(methyl methacrylate) (PMMA) films.

Because of the broad applicability of visible and IR absorption spectroscopy we expect this instrumentation to be useful for characterizing materials exhibiting nanoscale heterogeneity in composition and/or optical properties that are key for applications ranging from photovoltaics to therapeutics.

Recently, we integrated a table-top broadly tunable laser that exploits difference frequency generation in a GaSe crystal (laser B in figure 1) with a commercial PTIR setup to extend its spectral range from 1.55 µm to 16.0 µm (from 6450 cm^{-1} to 625 cm^{-1}) [18,21]. In this letter we couple our setup with an additional commercially available laser (laser C, figure 1) tunable in the VIS and NIR ranges. Laser C consists of a nanosecond Q-switched diode pumped Nd:YAG pump laser and an optical parametric

oscillator based on a beta barium borate nonlinear crystal integrated into a single enclosure. Three lasers are interfaced with the PTIR setup (Figure 1a) providing wavelengths from 400 nm to 16.0 μm. (see supporting information, SI). Light from lasers A and B is attenuated by a ZnSe wire grid polarizer (WGP-ZnSe) and light from laser C is attenuated by a WGP made of silicon nanowires (WGP-Si). Two motorized mirrors (M1 and M2) select the laser source and a polarization control module (PM), consisting of a set of three mirrors, can be inserted in the optical path to control light polarization at the sample [22,23]. Finally, the light is focused under the AFM tip by a ZnSe lens (L). The transmission of ZnSe limits the instrument spectral range to wavelengths ≥ 500 nm. Sample illumination is achieved by total internal reflection to minimize the direct light-tip interaction and requires preparing the sample on a transparent prism (ZnS in this work). A slightly modified prism holder was designed to enable data acquisition in the whole spectral range within the geometrical constraints of our setup.

The absorption of light pulses in the sample induces a rise in the local temperature and the thermal expansion of the sample which deflects the AFM cantilever. The cantilever deflection (figure 1b, inset), proportional to absorption [17], is read out using the AFM's photodetector synced to the laser pulse. The Fourier transformation of the signal (figure 1b) reveals the cantilever contact-resonance modes in the frequency domain. PTIR spectra are obtained by plotting the maximum cantilever deflection or the amplitude of one of the cantilever's modes as a function of wavelength while maintaining the AFM tip in a fixed location. Conversely, PTIR maps are obtained by plotting the PTIR signal as a function of sample location under fixed wavelength illumination.

In the mid-IR, the absorbed energy is converted into vibrational energy directly. In the visible and NIR the absorbed energy is converted initially into electronic excitation and later into vibrational energy via electro-vibrational coupling[24], on a timescale of few ps for dyes in PMMA matrices [25]. Vibrational excitations in molecular solids can be either: (i) localized to a chemical group (typically with higher frequencies, low-amplitude modes), (ii) localized on a particular molecule (typically with lower frequencies high-amplitude collective modes) or (iii) delocalized over several molecules in the form of phonons. Upon the absorption of an IR laser pulse, the energy of a localized mode (i) is rapidly redistributed to high amplitude low frequency modes (ii) because of the anharmonicity of the intramolecular potential and subsequently, is transferred to phonons on a sub-nanosecond timescale [25]. Whether the sample vibrational energy is excited directly (mid-IR) or indirectly (VIS-nIR) its excitation is much faster than the AFM feedback and the resulting thermal expansion is seen by the AFM cantilever as an impulsive loading [18].

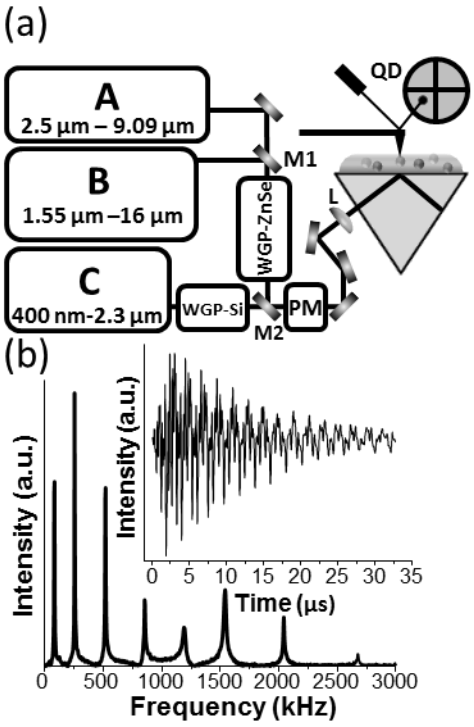

FIG. 1. (a) Diagram of PTIR set-up. (b) The Fourier transformation of the cantilever ring-down (inset) reveals the resonant oscillation modes induced in the cantilever.

Three samples (**S-1310**, **S-9578**, and **S-9658**) consisting of commercially available proprietary dyes dispersed in polymethyl methacrylate (PMMA) matrices were prepared on ZnS prisms. **S-1310** is a film with a thickness of 200 nm ± 15 nm, as determined by AFM. Uncertainties through the manuscript represent a single standard deviation. **S-9578** and **S-9658** consist of lines of PMMA-loaded dye with thickness of 350 nm ± 25 nm and 425 nm ± 25 nm, respectively. 1310 and 9578 dyes were miscible in PMMA but the 9658 dye was not and formed phase separated domains. To enable the comparison with macroscale spectra, bulk reference samples **R-1310**, **R-9578**, and **R-9658** were prepared on a glass substrate. Details on the sample preparation and data collection can be found in the SI.

PTIR absorption spectra in the VIS and NIR ranges (Figure 2a-c, red) closely resemble the extinction spectra of the bulk reference films (figure 2d-f, black) recorded with a UV-Vis spectrometer. Since the extinction spectra are the sum of both absorption and scattering but PTIR spectra are independent of scattering, the small differences between PTIR and reference spectra are attributed to scattering in the latter.

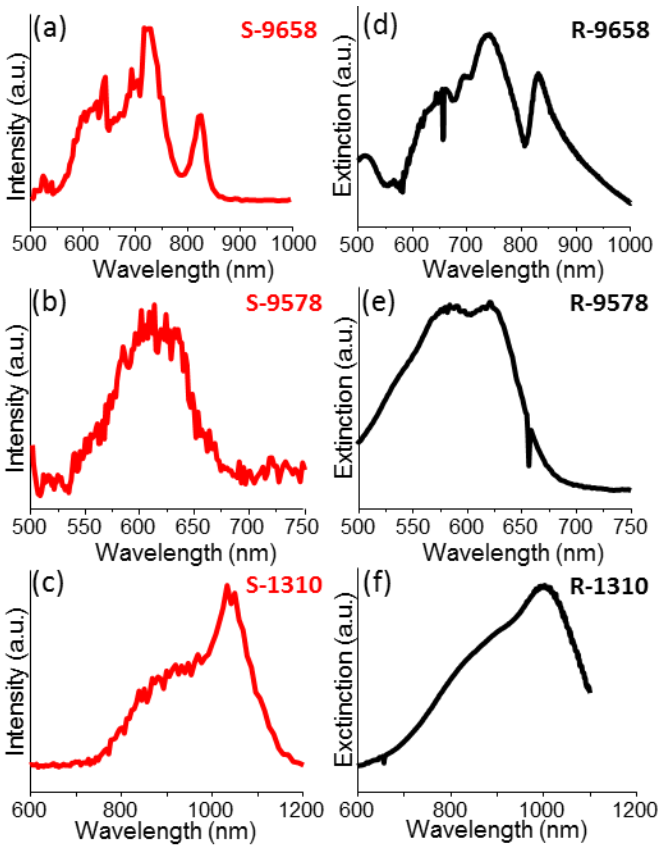

FIG. 2. PTIR spectra of **S-9658**, **S-9578**, and **S-1310** (a-c, red) and macroscale UV-Vis spectra (d-f, black) of the corresponding dye-loaded PMMA reference films.

The AFM topography image of **S-9658** (figure 3c) reveals protrusions in the PMMA matrix which are identified as the 9658 dye by their PTIR spectra (figure 3a red). In contrast, the PTIR spectra of the PMMA matrix show negligible absorption in the VIS/NIR range (figure 3a, black). Consistently, the PTIR absorption map at 725 nm highlights the sample heterogeneity revealing phase separated domains consisting of the 9658 dye within the PMMA matrix (figure 3d). In the mid-IR, the PTIR spectra of the dye particles (red, figure 3b) show a unique peak at 1316 cm^{-1} (7.60 µm) which we tentatively attribute to the C-N stretching of aromatic amines [26]. All other peaks are assigned to PMMA (see black spectrum in fig 3b, collected in PMMA matrix region) and suggest that some PMMA is present under the dye particles which is confirmed by the map of PMMA absorption at 1180 cm^{-1} (figure S1 of the SI). The absorption map of the dye C-N stretching (7.60 µm, figure 3e) essentially matches the map obtained with 725 nm illumination. Despite excitation wavelengths differing by more than one order of magnitude, both electronic and vibrational resonances identify the dye particles with nanoscale and wavelength-independent resolution.

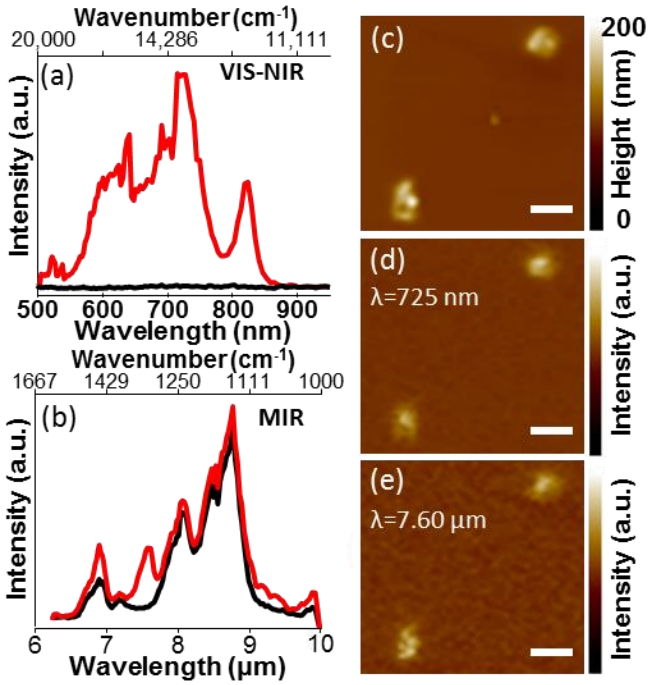

FIG. 3. (a) Visible/NIR PTIR spectra for **S-9658** collected on a dye particle (red) and on the PMMA matrix (black). (b) mid-IR PTIR spectra for **S-9658** collected on a dye particle (red) and on the PMMA matrix (black). (c) AFM height image of **S-9658.** (d) Corresponding PTIR absorption map at 725 nm. (e) PTIR absorption map at 1316 cm^{-1} (7.60 µm) corresponding to aromatic amine C-N stretching of the 9658 dye. Scale bars are 1 µm.

PTIR lateral resolution is typically estimated based on the comparison with topographic data and for thin samples was estimated as ≈ 100 nm [15,17,19,27]. In a related technique that relies on lasers with tunable repetition rates to match one of the AFM contact resonance frequencies, a resolution of ≈ 25 nm was reported based on the IR signal decay in comparison with topography [28].

The s-SNOM lateral resolution has been assessed by determining: the distance over which a feature in the optical signal falls [29,30], the number of pixels of a given size over which a feature vanishes [31], the ability to identify a structure's edge [32], and the full-width at half maximum (FWHM) of the optical signal [33]. Of the methods for assessing the PTIR or s-SNOM resolution, only the FWHM is an inherently unambiguous metric, and it is most useful for features smaller than the resolution limit. Comparisons of lateral resolution values in the PTIR and SNOM literature are difficult because estimates are typically carried out only at arbitrary points, thus lacking statistical analysis and uncertainties.

High resolution maps (10 nm pixel size) of **S-9658** were used to estimate the PTIR resolution. Figure 4a shows the height image recorded simultaneously with the 7.60 μm absorption map (Figure 4b). Figures 4c,d show height and 725 nm absorption maps, respectively, obtained in an earlier scan of the same particle. The **S-9658** may not be ideal for determining spatial resolution since the dye particle features do not vary abruptly on the length scale of the PTIR resolution. Therefore we validate the estimate of the PTIR spatial resolution using an independent measure – the topographic data recorded simultaneously. A limitation of this method is the variation of the particle-matrix physical overlap at their interface that can lead to estimates of the particle size from the topography to be larger or smaller than its intrinsic value (see below). However, for the sample studied here the discrepancy is small. Figure 4e shows normalized line profiles for height (black) and PTIR absorption at 7.60 μm (red) corresponding to the dashed lines in figure 4 a,b. The distance, *d*, over which the signal changes from 80 % to 20 % of the maximum is 80 nm for both PTIR and height signals. This measure provides the upper limit of the PTIR resolution on this sample. The FWHM of the PTIR signal is within 20 nm of the FWHM of the height signal. Additionally, the particle's extent determined by PTIR, is in good agreement with the height data (Figure 4e, inset). Contour plots for the PTIR signal (at 10 % of the maximum) for 7.60 μm and 725 nm excitation (red) are overlaid with height data (green) and appear orange in regions of overlap. The red regions represent areas where the PTIR signal extends beyond the particle extent as determined by the height maps. This can be ascribed to a portion of the particle that extends beneath the PMMA surface. Conversely, the green regions identify portions of the sample in which the PMMA bulges in proximity of the particle. The regions where the two signals are not perfectly overlapped extend radially by less than 100 nm (with the exception of loose dye debris noted by the white arrow in fig. 4e) and vanish at several locations. To quantify the resolution, the full-width at 10% of height ($FWTM_{height}$) and PTIR ($FWTM_{PTIR}$) maximum signals were compared for 20 vertical and 20 horizontal scan lines at each wavelength. $\left|FWTM_{height} - FWTM_{PTIR}\right|$ was 18 nm ± 24 nm at 7.60 μm, and 21 nm ± 18 nm at 725 nm. The uncertainties in the resolution are mostly determined by the variability in the particle-matrix interface. The ultimate PTIR resolution may be better than ≈ 20 nm but its assessment requires samples with sharper features. Theoretical models have suggested that for thick samples the PTIR resolution can be a function of the sample thermo-mechanical properties [34]; consequently this level of resolution may not be obtainable for every sample.

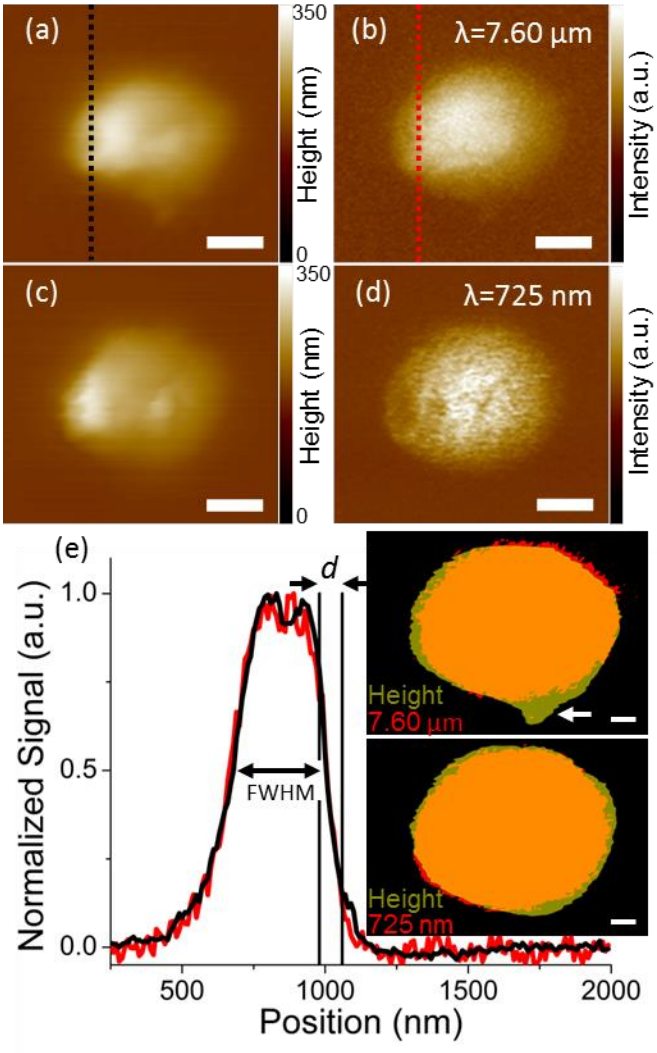

FIG. 4. (a, c) Consecutive height images (10 nm pixel size) of **S-9658**. (b) PTIR image at 7.60 µm recorded simultaneously with the height image in panel a. (d) PTIR image at 725 nm recorded simultaneously with the height image in panel c. (e) Line profiles (averaged over 5 lines) corresponding to the dashed lines in panel a (black) and c (red). The inset shows contour plots of the PTIR signal (red) overlaid with the height signal (green) at 10% of the signals' maxima. In the orange regions the two signals overlap. Scale bars are 250 nm in (a-d) and 100 nm in (e).

PTIR maps and spectra on **S-1310** and **S-9578** suggest that for these samples the dyes were homogeneously dispersed in the PMMA matrix up to a resolution of 100 nm. 1310 and 9578 dyes can thus impart their optical properties to PMMA films and could be used in applications requiring large optical absorption and homogeneity such as filters and safety glasses.

In summary, a wavelength-tunable laser was integrated into a modified PTIR commercial instrument extending its spectral range in the visible and NIR ranges for the first time. The resulting table-top setup enables the acquisition of absorption spectra and maps from 500 nm to 16.0 μm with ≈ 20 nm wavelength-independent spatial resolution. In the mid-IR, PTIR has already enabled the characterization of diverse samples such as polymers [19,20,22], bacteria [15,16], cells [35], drug nanocrystals [36], metal-organic frameworks [21], and plasmonic nanostructures [22,23]. We believe that the capability of providing correlated composition (mid-IR) and electronic absorption properties (VIS, NIR) with nanoscale resolution will be useful to characterize and engineer an even wider range of nanoscale materials and devices in fields such as photovoltaics, optoelectronic, theranostics and sensing.

Acknowledgement

A. C. acknowledges Lucian Hand of Altos Photonics for the useful discussion on the laser systems.

[1] J. Robertson, Philosophical Magazine B-Physics of Condensed Matter Statistical Mechanics Electronic Optical and Magnetic Properties **63**, 47 (1991).
[2] H. Schulz and M. Baranska, Vib. Spectrosc **43**, 13 (2007).
[3] I. W. Levin and R. Bhargava, Annu. Rev. Phys. Chem. **56**, 429 (2005).
[4] E. Abbe, Journal of the Royal Microscopical Society **3**, 790 (1883).
[5] S. W. Hell and J. Wichmann, Opt. Lett. **19**, 780 (1994).
[6] E. Betzig, G. H. Patterson, R. Sougrat, O. W. Lindwasser, S. Olenych, J. S. Bonifacino, M. W. Davidson, J. Lippincott-Schwartz, and H. F. Hess, Science **313**, 1642 (2006).
[7] M. J. Rust, M. Bates, and X. W. Zhuang, Nat Methods **3**, 793 (2006).
[8] F. Huth, M. Schnell, J. Wittborn, N. Ocelic, and R. Hillenbrand, Nat Mater **10**, 352 (2011).
[9] X. G. Xu, M. Rang, I. M. Craig, and M. B. Raschke, J. Phys. Chem. Lett. **3**, 1836 (2012).
[10] F. Keilmann, A. J. Huber, and R. Hillenbrand, J Infrared Millim Te **30**, 1255 (2009).
[11] H. A. Bechtel, E. A. Muller, R. L. Olmon, M. C. Martin, and M. B. Raschke, Proceedings of the National Academy of Sciences **111**, 7191 (2014).
[12] I. M. Craig, M. S. Taubman, A. S. Lea, M. C. Phillips, E. E. Josberger, and M. B. Raschke, Opt. Express **21**, 30401 (2013).
[13] A. Cvitkovic, N. Ocelic, and R. Hillenbrand, Opt. Express **15**, 8550 (2007).
[14] B. Knoll and F. Keilmann, Opt. Commun. **182**, 321 (2000).
[15] A. Dazzi, R. Prazeres, E. Glotin, and J. M. Ortega, Opt. Lett. **30**, 2388 (2005).
[16] A. Dazzi, R. Prazeres, F. Glotin, J. M. Ortega, M. Al-Sawaftah, and M. de Frutos, Ultramicroscopy **108**, 635 (2008).
[17] B. Lahiri, G. Holland, and A. Centrone, Small **9**, 439 (2013).
[18] A. M. Katzenmeyer, V. Aksyuk, and A. Centrone, Anal. Chem. **85**, 1972 (2013).
[19] J. R. Felts, K. Kjoller, M. Lo, C. B. Prater, and W. P. King, ACS Nano **6**, 8015 (2012).
[20] C. Marcott, M. Lo, K. Kjoller, C. Prater, and I. Noda, Appl. Spectrosc. **65**, 1145 (2011).
[21] A. M. Katzenmeyer, J. Canivet, G. Holland, D. Farrusseng, and A. Centrone, Angew. Chem. Int. Ed. **53**, 2852 (2014).

[22] B. Lahiri, G. Holland, V. Aksyuk, and A. Centrone, Nano Lett. **13**, 3218 (2013).
[23] A. M. Katzenmeyer, J. Chae, R. Kasica, G. Holland, B. Lahiri, and A. Centrone, Adv. Opt. Mater. **2**, 718 (2014).
[24] S. Link and M. A. El-Sayed, Annu. Rev. Phys. Chem. **54**, 331 (2003).
[25] S. Chen, I. Y. S. Lee, W. A. Tolbert, X. Wen, and D. D. Dlott, The Journal of Physical Chemistry **96**, 7178 (1992).
[26] L. J. Bellamy, *The Infra-red Spectra of Complex Molecules* (John Wiley & Sons, Inc., New York, 1980), 2nd edn.
[27] C. Mayet, A. Dazzi, R. Prazeres, E. Allot, E. Glotin, and J. M. Ortega, Opt. Lett. **33**, 1611 (2008).
[28] F. Lu, M. Jin, and M. A. Belkin, Nat Photon **8**, 307 (2014).
[29] M. B. Raschke, L. Molina, T. Elsaesser, D. H. Kim, W. Knoll, and K. Hinrichs, ChemPhysChem **6**, 2197 (2005).
[30] F. Keilmann and R. Hillenbrand, Philos T Roy Soc A **362**, 787 (2004).
[31] F. Huth, A. Govyadinov, S. Amarie, W. Nuansing, F. Keilmann, and R. Hillenbrand, Nano Lett. **12**, 3973 (2012).
[32] R. Hillenbrand and F. Keilmann, Phys. Rev. Lett. **85**, 3029 (2000).
[33] A. Hartschuh, E. J. Sanchez, X. S. Xie, and L. Novotny, Phys. Rev. Lett. **90**, 095503 (2003).
[34] A. Dazzi, in *Thermal Nanosystems and Nanomaterials* (Springer, 2009), pp. 469.
[35] C. Mayet, A. Dazzi, R. Prazeres, F. Allot, F. Glotin, and J. M. Ortega, Opt. Lett. **33**, 1611 (2008).
[36] A. J. Harrison, E. A. Bilgili, S. P. Beaudoin, and L. S. Tayor, Anal. Chem. **85**, 11449 (2013).

Supporting information for:

Absorption Spectroscopy and Imaging from the Visible through Mid-Infrared with 20 nm Resolution.

Aaron M. Katzenmeyer, Glenn Holland, Kevin Kjoller and Andrea Centrone[*]

[1]Center for Nanoscale Science and Technology, National Institute of Standards and Technology, 100 Bureau Drive, Gaithersburg, Maryland 20899, United States.
[*]E-mail: andrea.centrone@nist.gov

[2]Anasys Instruments, Inc., 325 Chapala Street, Santa Barbara, California 93101, United States.

Experimental Details

Commercial Si probes with the following nominal specifications were used for all PTIR experiments - frequency: 17 kHz, spring constant: 0.33 N/m, radius of curvature: 6 nm. PTIR maps were recorded with moderate (100 nm) or high (10 nm) pixel resolution by averaging the intensity of 64 or 32 laser pulses, respectively. PTIR spectra were recorded by averaging the intensity for 256 laser pulses at each wavelength and by sweeping the wavelength at intervals of 4 cm^{-1} (mid-IR) or 80 cm^{-1} (visible and near-IR). The PTIR intensity was normalized with respect to the laser power spectrum (background) measured with a pyroelectric detector (inserted in place of the sample) by averaging 2048 pulses at each wavelength.

To obtain correlated topographic and chemical images, the pixel size in the AFM height and PTIR images must be identical. If n^{pixel} (pixel/line) is the number of pixels in the fast AFM scanning direction and v is the AFM scan rate (lines/s), the AFM height pixel rate (ξ_{AFM}, pixels per second) is given by:

$$\xi_{AFM} = 2 \cdot n^{pixel} \cdot v \qquad (1)$$

To obtain the maximum resolution ξ_{AFM} should be equal to the PTIR pixel rate (ξ_{PTIR}) defined as follows:

$$\xi_{PTIR} = \frac{\omega}{n^{avg-pulses}} \quad (2)$$

Where ω is the laser (fixed) repetition rate (1 kHz for laser A and B, 0.8 kHz for laser C) and $n^{avg\text{-}pulses}$ is the number of pulses that are averaged for each pixel (32 or 64 in this work). If this condition is not met the pixel size of the PTIR chemical image will differ from the pixel size in the height image making correlations difficult if the two numbers are appreciably different.

Lasers Description:

PTIR experiments were carried out using a commercial PTIR setup which consists of an AFM microscope operating in contact mode and a tunable OPO laser source (laser A in Figure 1 of the main text). A second tunable DFG laser system (laser B in figure 1) was integrated with the setup and described previously [1]. A third OPO laser (Laser C in figure 1) tunable in the VIS and NIR ranges was integrated in this work.

Laser A consists of a Q-switched diode pumped Nd:YAG laser (1064 nm), one optical parametric oscillator (OPO) based on a periodically poled lithium niobate (PPLN) crystal and a second OPO based on a noncritically phase-matched ZnGeP2 (ZGP) crystal. Laser A emits 10 ns pulses with a 1 kHz repetition rate and line widths between 5 cm−1 and 16 cm−1 depending on the wavelength. Laser A is tunable between 2.5 μm and 9.09 μm. Additional details can be found elsewhere [1].

Laser B consists of a modelocked picosecond laser pump which provides a pulse train for driving a synchronously pumped optical parametric oscillator (SOPO) and a single pulse for pumping an optical parametric amplifier (OPA) and a difference frequency generation (DFG) stage. The SOPO is designed such that the cavity round-trip time is matched to the interpulse spacing in the pulse train. Laser B has a tunable output from 1.55 μm to 16.00 μm with 1 kHz repetition rate, 100 ps pulses, 0.5 cm−1 line width and energy per pulse up to 500 μJ. Dichroic mirrors or absorptive filters, depending on the wavelength, are used to cut unwanted spectral lines, so only a single wavelength is present at a time at the laser output. Additional details can be found elsewhere [1].

Laser C consists of a nanosecond Q-switched diode pumped Nd:YAG pump laser and an optical parametric oscillator based on a beta barium borate non-linear crystal integrated into a single enclosure. Laser C emits 10 ns pulses with < 1 nm line width at up to 1 kHz (0.8 KHz in this work) in the range from 400 nm to 2300 nm.

Sample Preparation

For each sample a saturated solution was prepared by dissolving the dye in PMMA (495,000 M_W) anisole solution (4% w/w). Sample **S-1310** was obtained by spin casting the dye-PMMA solution (50 Hz)

and annealing it (170°C oven, 30 min) resulting in a film with a thickness of 200 nm ± 15 nm, as determined by AFM. Uncertainties through the manuscript represent a single standard deviation. **S-9578** and **S-9658** were prepared by directly writing dye-loaded PMMA lines with a probe (angle-cut 255 µm diameter bus bar wire, see e.g. , [2])

by dragging a droplet of solution placed on the edge of the prism with the aid of an optical microscope. **S-9578** and **S-9658** consist of lines with a thickness of 350 nm ± 25 nm and 425 nm ± 25 nm, respectively. To enable the comparison with macroscale spectra, bulk reference samples **R-1310**, **R-9578**, and **R-9658** were prepared by placing a drop of dye-loaded PMMA solutions on a glass cover slip. The reference samples were then annealed on a hot plate (180 °C, 2 min) and characterized with a UV-Vis spectrometer.

Proprietary dye molecules were acquired from Adam Gates & Company, LLC and used a received. (The materials used in this paper require the identification of a commercial product and its supplier. The inclusion of such information should in no way be construed as indicating that such product or supplier is endorsed by NIST or is recommended by NIST or that is necessarily the best material for the purpose described.)

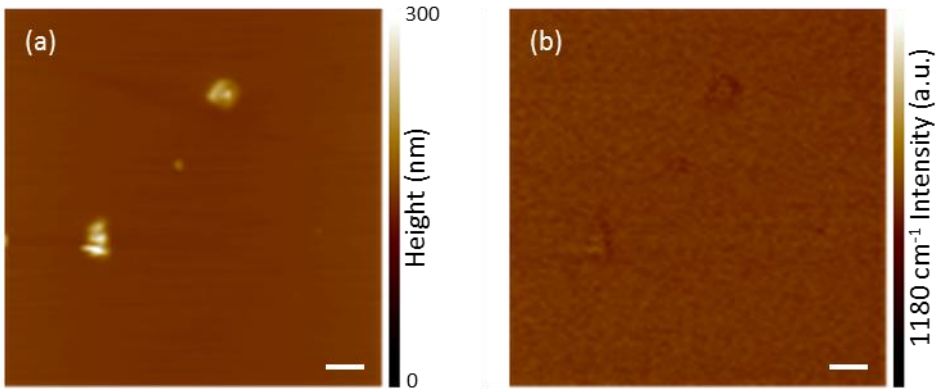

Figure S1. (a) Height and (b) PTIR image recorded in correspondence with the PMMA absorption at 1180 cm^{-1}. Compare to figure 3 of the main text. Little contrast at the locations of the particles is observed as the PMMA matrix underlaps the dye particles observed in the height image. Scale bars are 1 µm.

[1] A. M. Katzenmeyer, V. Aksyuk, and A. Centrone, Anal. Chem. 85, 1972 (2013).

[2] S. A. Harfenist, S. D. Cambron, E. W. Nelson, S. M. Berry, A. W. Isham, M. M. Crain, K. M. Walsh, R. S. Keynton, and R. W. Cohn, Nano Lett. 4, 1931 (2004).